Water Vapor Retrieval Over Cloud Cover Area on Land Using AMSR-E and MODIS

Dabin Ji and Jiancheng Shi, *Fellow*, *IEEE*

***Abstract*—This study mainly discusses atmospheric water vapor retrieval over cloud cover area on land with the help of a newly developed surface emissivity parameter estimation method in microwave bands. In the retrieval method, the atmospheric water vapor sensitivity parameter—ratio of brightness temperature polarization difference at frequencies 18.7 and 23.8 GHz ($\Delta \mathrm{Tb}_{18.7}/\Delta \mathrm{Tb}_{23.8}$)—is used to retrieve water vapor, and the surface emissivity parameter—ratio of surface emissivity polarization difference at frequencies 18.7 and 23.8 GHz ($\Delta\varepsilon_{18.7}/\Delta\varepsilon_{23.8}$) that corresponds to $\Delta \mathrm{Tb}_{18.7}/\Delta \mathrm{Tb}_{23.8}$—is a key parameter that affects the final precision of retrieved atmosphere water vapor. In order to estimate $\Delta\varepsilon_{18.7}/\Delta\varepsilon_{23.8}$ in cloudy condition, we first estimated the value of $\Delta\varepsilon_{18.7}/\Delta\varepsilon_{23.8}$ in clear condition using Advanced Microwave Scanning Radiometer for EOS (AMSR-E) brightness temperature and related MODIS atmospheric products. At the same time, it was found that gradient information derived separately from $\Delta \mathrm{Tb}_{18.7}/\Delta \mathrm{Tb}_{23.8}$ and $\Delta\varepsilon_{18.7}/\Delta\varepsilon_{23.8}$ has very good correlation with each other. Based on this good correlation, the $\Delta\varepsilon_{18.7}/\Delta\varepsilon_{23.8}$ in cloudy condition was estimated using corresponding $\Delta \mathrm{Tb}_{18.7}/\Delta \mathrm{Tb}_{23.8}$ and adjacent 8 days $\Delta\varepsilon_{18.7}/\Delta\varepsilon_{23.8}$ in clear condition. With the estimated $\Delta\varepsilon_{18.7}/\Delta\varepsilon_{23.8}$, we retrieved atmospheric column water vapor using lookup table method in cloudy condition over land. As a validation source data, the SuomiNet GPS-retrieved precipitable water (PW) vapor is used to validate the retrieved water vapor in this study. According to validation, the correlation coefficient of the two is 0.94 and the root-mean-square-error (RMSE) is 4.85 mm. It is a great improvement in water vapor retrieval using microwave in cloud cover area on land.**

***Index Terms*—Advanced Microwave Scanning Radiometer for EOS (AMSR-E), microwave, surface emissivity, water vapor.**

I. Introduction

ATMOSPHERIC water vapor plays an important role in the Earth system. It contributes to the whole Earth in several ways. First, atmospheric water vapor is a key parameter in hydrologic cycle. Water vapor evaporates from land or sea surface, then condenses to form clouds and blown to other places by wind, finally falling to the Earth surface in the form of precipitation [1]. Second, atmospheric water vapor is an important energy carrier between surface and atmosphere. It absorbs heat from the Sun in the evaporation process, and put the heat into the air when condensing into clouds or precipitation. These two processes are important ways to transfer energy from the Earth surface to the air [1]. Third, atmospheric water vapor is also an important kind of greenhouse gases in the atmosphere besides carbon dioxide and methane. It absorbs long wave radiation emitted from the Earth surface and heats the air. Without these greenhouse gases, the Earth surface will become very cold [1]. So, it is very important to know the temporal and spatial distributions of water vapor all over the globe.

Remote sensing provides an effective way to retrieve atmospheric water vapor in large area. Currently, there are mainly two types of remote sensing data that are used to retrieve atmospheric water vapor. One is optical remote sensing data. The other is microwave data.

Near infrared data and thermal infrared data are mainly used to retrieve water vapor in optical remote sensing. The algorithms using these two types of data to retrieve water vapor are currently in operation. In near infrared, the ratio of water vapor absorbing channels centered near 0.905, 0.936, and $0.940\ \mu\mathrm{m}$ with atmospheric window channels at 0.865 and $1.24\ \mu\mathrm{m}$ are used to retrieve water vapor; typical errors in the derived water vapor values are in the range between 5% and 10% [2], [3]. In thermal infrared, single channel [4] and two adjacent channels in the infrared split-window region near $10-12\ \mu\mathrm{m}$ [5]–[8] are usually used to retrieve water vapor. These two types of algorithm in optical remote sensing can provide atmospheric column water vapor with high precision in clear condition. When clouds are present, the algorithm using near infrared remote sensing data can only provide water vapor information on the Sun–cloud–sensor path over optically thick cloud or water vapor information above and within thin clouds. They are not able to provide water vapor information between cloud and the Earth surface because of its short wavelength. As a complement of optical remote sensing of atmospheric water vapor, passive microwave has the ability to provide the way to retrieve water vapor in cloudy condition due to its long wavelength compared with the size of cloud particles.

There are various atmospheric water vapor retrieval algorithms using passive microwave. Generally, these algorithms can be categorized into four main groups: statistical algorithms, semi-statistical algorithms, physical algorithms, and neural network algorithms. The statistical algorithms retrieve atmospheric water vapor using the relationship derived between ground-based observed data and one or multi-bands of space-based passive microwave radiometer data [9]–[11]. The advantage of such algorithms is simple and easy to achieve. However, the relationship used to retrieve water vapor is greatly affected by the quality of selected data. When applied in global scale, the

Manuscript received September 13, 2013; revised November 24, 2013; accepted December 29, 2013. Date of publication January 27, 2014; date of current version August 21, 2014. This work was supported in part by the CAS/SAFEA International Partnership Program for Creative Research Teams under Grant KZZD-EW-TZ-09, in part by National Natural Science Foundation of China under Grant 40930530, and in part by National Natural Science Foundation of China under Grant 41371354. *(Corresponding author: J. Shi.)*

The authors are with the State Key Laboratory of Remote Sensing Science, Institute of Remote Sensing and Digital Earth, Chinese Academy of Sciences, Beijing 100101, China (e-mail: dabinj@gmail.com; jshi@irsa.ac.cn).

Color versions of one or more of the figures in this paper are available online at http://ieeexplore.ieee.org.

Digital Object Identifier 10.1109/JSTARS.2014.2298979

algorithms may introduce great errors in local area due to the lack of physical constraints. Compared with statistical algorithms, the semi-statistical algorithms introduce constraints of radiative transfer model when building the regression relationship of atmospheric water vapor and brightness temperature from microwave radiometer [12]–[14]. This can greatly reduce errors in local regions for global scale algorithms. The disadvantage of the semi-statistical algorithms is that some environmental variables may be improperly introduced or ignored in the retrieval and cause errors in the retrieved water vapor. The third group is physical algorithms that rely solely on radiative transfer equation in the retrieval [15], [16]. Compared to the aforementioned two groups of algorithms, the physical algorithms have definite physical meaning. However, complexity of radiative transfer equation makes it difficult to be widely used. Simplification and assumption of the radiative transfer equation in actual retrieval limit the ability of physical algorithms. The fourth group is neural network algorithms. Here, we separate it from statistical algorithms. The reason is the way it is different from common statistical algorithms in building relationship between retrieved variables and observed variables. Neural network techniques have already proved very successful in the developments of computationally efficient inversion methods for satellite data and for geophysical applications [17], [18]. They are well adapted to solve nonlinear problems and are especially designed to capitalize on the inherent statistical relationships among the retrieved parameters [17]. The problem of neural network is that it is not able to explain its reasoning process and theoretical basis and it cannot work very well when the data are not sufficiently provided.

Most of these algorithms using microwave radiation work very well over ocean area. However, only a few of these studies have put efforts on the retrieval of atmosphere parameters from microwave observations over land. The main reason for this situation is that the ocean surface has a low microwave emissivity (about 0.5) that produces good contrast of atmospheric phenomena against a low-brightness temperature background; the land surface emissivity is usually close to unity, making atmospheric features much more difficult to identify against a higher brightness temperature background [17]. In [19], a new method was proposed to retrieve cloud liquid water over land using Special Sensor Microwave Imager (SSM/I), and [20] improved this algorithm with a normalized polarization difference parameter. They estimated the surface emissivity with the help of collocated infrared measurement on GOES-7 in clear condition. For cloudy condition, they estimated the surface emissivity using an average of adjacent 7-day period clear-conditioned surface emissivity. It may introduce great error to the estimated surface emissivity in cloudy condition when there is rain precipitation event during the adjacent 7-day period. In [12], a new method was proposed to estimate water vapor using the observation from the Advanced Microwave Scanning Radiometer for EOS (AMSR-E) satellite instrument. The method retrieved atmospheric water vapor using a water vapor sensitivity parameter—the ratio of the AMSR-E polarization-difference signals at 18.7 and 23.8 GHz ($\Delta \mathrm{Tb}_{23.8}/\Delta \mathrm{Tb}_{18.7}$). However, the problem is the surface emissivity parameter—the ratio of surface emissivity polarization difference at 18.7 and 23.8 GHz ($\Delta\varepsilon_{23.8}/\Delta\varepsilon_{18.7}$) was assumed to 1 in the retrieval. Actually, according to our calculation, the $\Delta\varepsilon_{23.8}/\Delta\varepsilon_{18.7}$ changes over seasons and different surface types. The assumption may introduce error to the retrieved atmospheric water vapor.

In this study, we propose a new method to estimate the surface emissivity parameter—$\Delta\varepsilon_{18.7}/\Delta\varepsilon_{23.8}$ in cloudy condition, and then it is used in the retrieval of atmospheric water vapor according to the sensitivity parameter—$\Delta \mathrm{Tb}_{18.7}/\Delta \mathrm{Tb}_{23.8}$ with the help of a lookup table technology. The lookup table is build by a 1-Dimensional Microwave Radiative Transfer Model (1-DMWRTM) [21], [22]. As a validation, SuomiNet GPS observed water vapor data [23] are used to validate to the retrieved water vapor. Section II describes the data used in the retrieval algorithm. Section III shows the basic theory of the algorithm and the method of estimating surface emissivity parameter in cloudy condition. Section IV is the validation part of this algorithm and Section V concludes this study.

II. Data Used in Retrieval

In the retrieval, four types of data are used. These include AMSR-E brightness temperature, MODIS products (MODIS surface temperature product, MYD11; MODIS cloud mask product, MYD35; MODIS water vapor product, MYD05; and MODIS cloud product, MYD06), radiosonde observation, and SuomiNet GPS observation.

The AMSR-E is a 12 channel, 6 frequency total power passive microwave radiometer system onboard the AQUA satellite. It measures brightness temperatures at frequencies 6.925, 10.65, 18.7, 23.8, 36.5, and 89.0 GHz. Vertically and horizontally polarized measurements are taken at all channels [24]. Only brightness temperature at frequencies 18.7 and 23.8 GHz is used for retrieval in this study. All these brightness temperatures are corrected by Earth incidence angle in order to retrieve the vertical column atmospheric water vapor or PW.

MODIS is another sensor onboard AQUA. As both AMSR-E and MODIS are onboard the same satellite, data from these two sensors can be easily matched in spatial and temporal scale. In the retrieval algorithm of this paper, MODIS water vapor and surface temperature product in clear sky are used to estimate $\Delta\varepsilon_{18.7}/\Delta\varepsilon_{23.8}$; MODIS cloud mask product is mainly used to identify cloud existence, and MODIS cloud product is used for cloud effect correction in the retrieval.

The radiosonde observations were derived from U.S. Southern Great Plains, in 2007. Four types of profiles are included in the observations: height, relative humidity, temperature, and pressure, which are used to build lookup table used to calculate emissivity and retrieve water vapor.

The SuomiNet GPS observations are used as validation data for the retrieved water vapor. SuomiNet is an international network of GPS receivers. The goal of SuomiNet is to make large amounts of spatially and temporally dense GPS-sensed PW vapor data widely available in real time, for academic research and education [23]. PW from GPS is calculated as the product of the zenith delay and a conversion factor [25]. The accuracy of GPS-sensed PW by this method is better than 2 mm [23], [25].

III. Algorithm Description

The algorithm theoretical basis is derived from the integrated radiative transfer equation, which is detailed in Section III-A. It explains why we use $\Delta\mathrm{Tb}_{18.7}/\Delta\mathrm{Tb}_{23.8}$ to retrieve water vapor. According to the description in Section III-A, the surface emissivity parameter $\Delta\varepsilon_{18.7}/\Delta\varepsilon_{23.8}$ is a key surface boundary parameter in the retrieval, and cloud liquid water also makes contribution to the value of $\Delta\mathrm{Tb}_{18.7}/\Delta\mathrm{Tb}_{23.8}$ besides water vapor. These two parameters are discussed in Sections III-B and III-C, respectively. In the end, Section III-D gives an overall description of the water vapor retrieval algorithm.

A. Basic Theory

The theory basis for water vapor retrieval in this study is atmospheric radiative transfer equation. Part of the description of the theory basis is also discussed in the previous study [26]. The integrated radiative transfer equation for a nonscattering, plane-parallel atmosphere with a non-blackbody surface boundary condition can be expressed as follows [19], [27]:

$$\begin{aligned}\mathrm{Tb}(0)_q^v &= \varepsilon_q^v T_s t_v(p_s,0) + \int_{p_s}^{0} T(p)\frac{\partial t_v(p,0)}{\partial p}dp \\ &\quad + (1-\varepsilon_q^v)[t_v(p_s,0)]^2\int_{p_s}^{0}\frac{T(p)}{[t_v(p,0)]^2}\frac{\partial t_v(p,0)}{\partial p}dp \\ &\quad + (1-\varepsilon_q^v)[t_v(p_s,0)]^2 T_{\mathrm{space}} \qquad (1)\end{aligned}$$

where $\mathrm{Tb}(0)_q^\nu$ is the upward brightness temperature observed by the satellite at pressure $p=0$, at the frequency ν, q represents polarization state vertical (V) or horizontal (H); ε_q^ν is the surface emissivity at frequency ν and polarization state q; T_s is the surface temperature, the subscript s denotes surface value; $t(p,0)$ is the atmospheric transmittance for a layer between pressure level p and $p=0$; and $T_{\mathrm{space}}=2.7$ K is cosmic background temperature.

The polarization difference of brightness temperature at a frequency can be calculated according to (1)

$$\begin{aligned}\Delta\mathrm{Tb}_v &= \mathrm{Tb}_V^v - \mathrm{Tb}_H^v = (\varepsilon_V^v-\varepsilon_H^v)T_s t(p_s,0) \\ &\quad - (\varepsilon_V^v-\varepsilon_H^v)[t(p_s,0)]^2\int_{p_s}^{0}\frac{T(p)}{[t(p,0)]^2}\frac{\partial t(p,0)}{\partial p}dp \\ &\quad - (\varepsilon_V^v-\varepsilon_H^v)[t(p_s,0)]^2 T_{\mathrm{space}} \qquad (2)\end{aligned}$$

where Tb_V^ν and Tb_H^ν are brightness temperature at frequency ν for vertical and horizontal polarization, respectively, ε_V^ν and ε_H^ν are surface emissivity at frequency ν for vertical and horizontal polarization, respectively.

For microwave frequencies between 18 and 89 GHz, brightness temperature received by sensor can be affected by water vapor, cloud liquid water, and rain in the atmosphere. In order to retrieve water vapor in the atmosphere, proper frequency or frequencies combination should be selected to suppress other information and highlight the information of water vapor. According to former research, the ratio of polarization difference of brightness temperature at frequencies 18.7 and 23.8 GHz ($\Delta\mathrm{Tb}_{18.7}/\Delta\mathrm{Tb}_{23.8}$) is sensitive to water vapor and less sensitive to other information in atmosphere [12], [14]. So, (3) can be deduced from (2)

$$\begin{aligned}\frac{\Delta\mathrm{Tb}_{18.7}}{\Delta\mathrm{Tb}_{23.8}} &= \frac{\Delta\varepsilon_{18.7}}{\Delta\varepsilon_{23.8}} \\ &\quad\cdot\frac{T_s t_{18.7} - t_{18.7}^2\int_{p_s}^{0}\frac{T(p)}{t_{18.7}^2(p,0)}\cdot\frac{\partial t_{18.7}(p,0)}{\partial p}dp - t_{18.7}^2 T_{\mathrm{space}}}{T_s t_{23.8} - t_{23.8}^2\int_{p_s}^{0}\frac{T(p)}{t_{23.8}^2(p,0)}\cdot\frac{\partial t_{23.8}(p,0)}{\partial p}dp - t_{23.8}^2 T_{\mathrm{space}}} \\ &= \frac{\Delta\varepsilon_{18.7}}{\Delta\varepsilon_{23.8}}\cdot f(T_s,wv) \qquad (3)\end{aligned}$$

where $\Delta\varepsilon_\nu = \varepsilon_V^\nu - \varepsilon_H^\nu$; $f(T_s,\mathrm{wv})$ is a function of surface temperature and water vapor.

According to (3), from the measurement of $\Delta\mathrm{Tb}_{18.7}/\Delta\mathrm{Tb}_{23.8}$ using AMSR-E brightness temperature, if $\Delta\varepsilon_{18.7}/\Delta\varepsilon_{23.8}$ and surface temperature T_S are known, then water vapor can be estimated. T_S is estimated using (4) and the precision is 4.5 K [28]

$$T_s = 1.11\mathrm{Tb}_{36.5} - 15.2, \quad \text{where } \mathrm{Tb}_{36.5\mathrm{V}} > 259.8\ \mathrm{K} \qquad (4)$$

where $\mathrm{Tb}_{36.5\mathrm{V}}$ is AMSR-E vertical polarization brightness temperature data at frequency 36.5 GHz. However, due to application limitation, (4) is not suitable for area with low surface temperature. For these areas, the surface temperature is estimated using average value of adjacent 7 days surface temperature retrieved from MODIS in clear condition. An error of 10 K in T_S would produce an atmospheric water vapor retrieval error of only 0.07 mm [12]. It is acceptable for the estimation of surface temperature T_S with a reasonable accuracy.

In (3), $\Delta\varepsilon_{18.7}/\Delta\varepsilon_{23.8}$ is an important parameter in the retrieval of water vapor. In pioneer research, $\Delta\varepsilon_{18.7}/\Delta\varepsilon_{23.8}$ is usually set as a constant for the sake of simplification [12], [14]. However, $\Delta\varepsilon_{18.7}/\Delta\varepsilon_{23.8}$ changes with different seasons and surface types according to our analysis in Fig. 1. It may introduce great errors if the variation in $\Delta\varepsilon_{18.7}/\Delta\varepsilon_{23.8}$ is ignored. The detail of estimation of $\Delta\varepsilon_{18.7}/\Delta\varepsilon_{23.8}$ and the analysis of its spatial and temporal variation are mainly discussed in Section III-B.

B. Surface Parameter Estimation

In water vapor retrieval, $\Delta\varepsilon_{18.7}/\Delta\varepsilon_{23.8}$ is an important surface parameter. In this section, this surface parameter in clear condition is first estimated using AMSR-E brightness data and MODIS water vapor and surface temperature product, and then, $\Delta\varepsilon_{18.7}/\Delta\varepsilon_{23.8}$ in cloudy condition is estimated using the adjacent 8 days data of $\Delta\varepsilon_{18.7}/\Delta\varepsilon_{23.8}$ in clear condition. The theory to estimate these surface parameters in clear condition is based on (3). According to (3), if $\Delta\mathrm{Tb}_{18.7}/\Delta\mathrm{Tb}_{23.8}$, T_S, and water vapor are known, $\Delta\varepsilon_{18.7}/\Delta\varepsilon_{23.8}$ can be estimated. Prior to the estimation, a sensitivity analysis is performed using 1-DMWRTM. The data used in the analysis are atmospheric profiles from radiosonde observations derived from U.S. Southern Great Plains, in 2007. Fig. 1 shows the sensitivity of the simulation. Fig. 1(a) shows the sensitivity of $\Delta\mathrm{Tb}_{18.7}/\Delta\mathrm{Tb}_{23.8}$ to $\Delta\varepsilon_{18.7}/\Delta\varepsilon_{23.8}$ at different water vapor contents, when surface temperature equals 300 K. According to Fig. 1, the slope increases as the water vapor

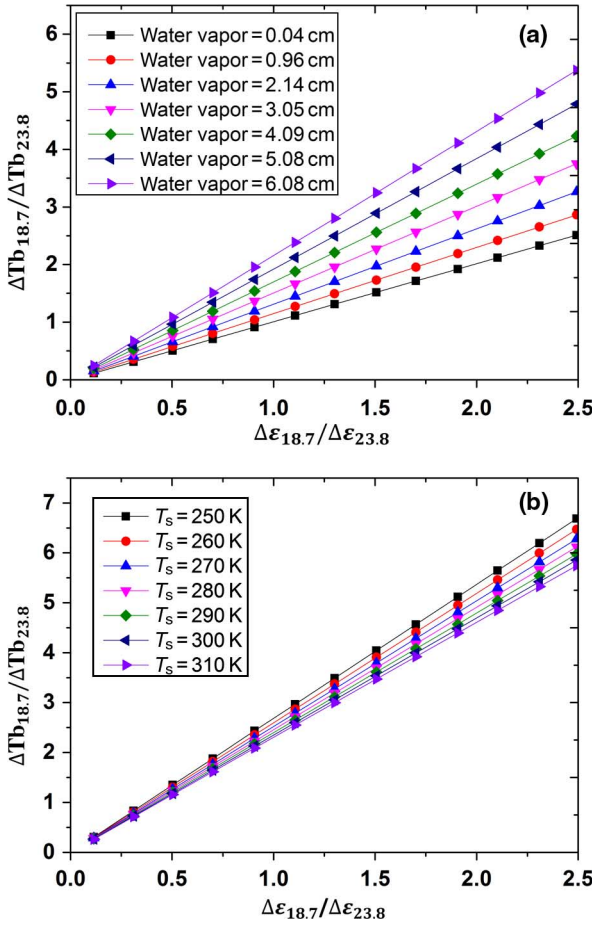

Fig. 1. (a) Sensitivity of $\Delta\mathrm{Tb}_{18.7}/\Delta\mathrm{Tb}_{23.8}$ to $\Delta\varepsilon_{18.7}/\Delta\varepsilon_{23.8}$ at different water vapor contents, when surface temperature equals to 300 K. (b) Sensitivity of $\Delta\mathrm{Tb}_{18.7}/\Delta\mathrm{Tb}_{23.8}$ to $\Delta\varepsilon_{18.7}/\Delta\varepsilon_{23.8}$ at different surface temperatures, when atmospheric water vapor content is 7.18 cm.

content getting larger and larger. Fig. 1(b) shows the sensitivity of $\Delta\mathrm{Tb}_{18.7}/\Delta\mathrm{Tb}_{23.8}$ to $\Delta\varepsilon_{18.7}/\Delta\varepsilon_{23.8}$ at different surface temperatures, when water vapor content is 7.18 cm. Although the effect of surface temperature to slope in Fig. 1 is not as much as that of the water vapor, the effect of surface temperature should not be ignored, the reason is that a variation of 10 K in surface temperature would produce a maximum change of 0.05 in $\Delta\varepsilon_{18.7}/\Delta\varepsilon_{23.8}$. On the whole, water vapor and surface temperature are the key parameters to estimate $\Delta\varepsilon_{18.7}/\Delta\varepsilon_{23.8}$ in clear condition.

Data used to estimate $\Delta\varepsilon_{18.7}/\Delta\varepsilon_{23.8}$ in clear condition include atmosphere profiles from radiosonde observation, AMSR-E brightness temperatures, and their corresponding MODIS water vapor and surface temperature products (MYD05 and MYD11). As a preprocess, the AMSR-E brightness temperature and MODIS products are re-projected into $0.25^\circ \times 0.25^\circ$ grid image, both types of the data match very well in temporal and spatial scale, because they are onboard in the same satellite AQUA.

The method used in estimating surface parameters is a lookup table technology. The lookup table is built using 1-DMWRTM, and it contains four fields: surface temperature, water vapor content, $\Delta\varepsilon_{18.7}/\Delta\varepsilon_{23.8}$, and $\Delta\mathrm{Tb}_{18.7}/\Delta\mathrm{Tb}_{23.8}$. Based on the lookup table, $\Delta\varepsilon_{18.7}/\Delta\varepsilon_{23.8}$ can be estimated using surface temperature, water vapor, and $\Delta\mathrm{Tb}_{18.7}/\Delta\mathrm{Tb}_{23.8}$ on each grid in clear condition.

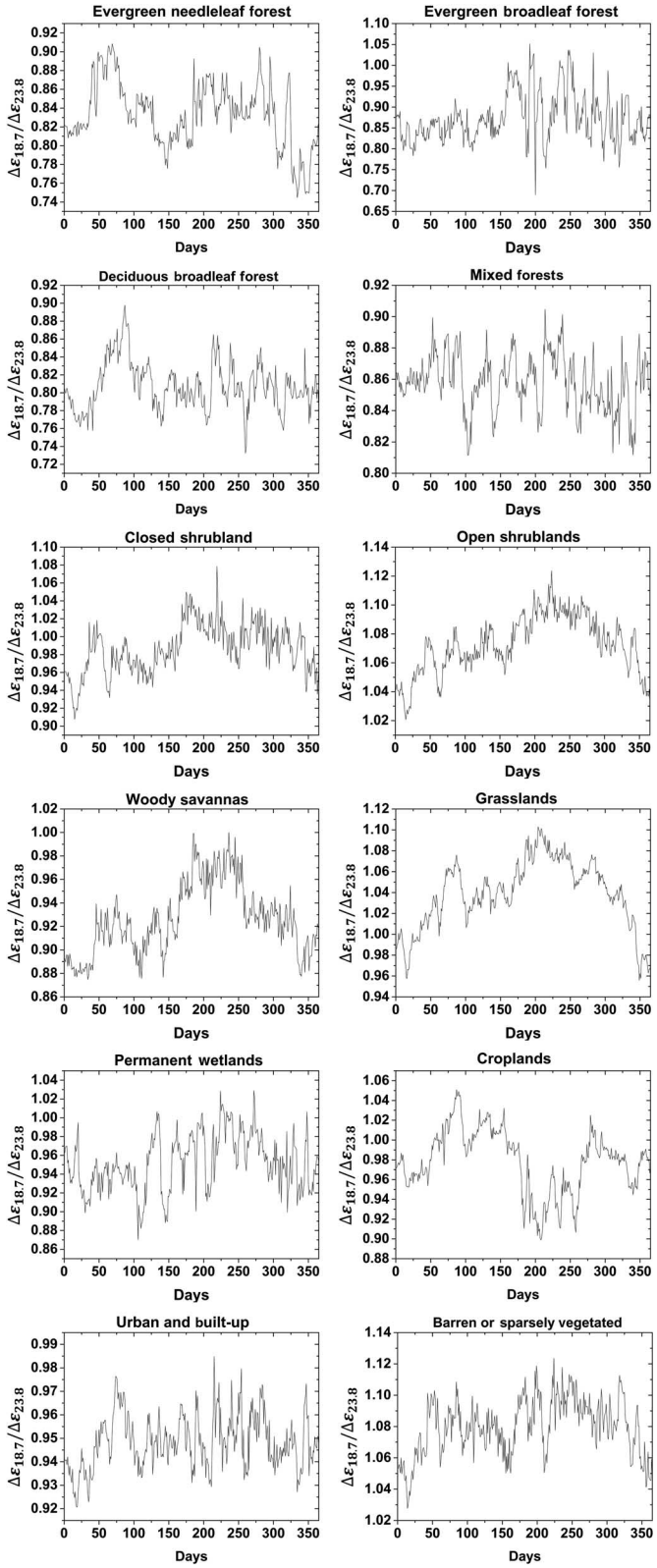

Fig. 2. Time series of mean $\Delta\varepsilon_{18.7}/\Delta\varepsilon_{23.8}$ of different land surface types in USA in a year.

As an analysis of temporal variability, the estimated $\Delta\varepsilon_{18.7}/\Delta\varepsilon_{23.8}$ in clear condition using lookup table method is used in time series analysis. Fig. 2 shows a time series plots of $\Delta\varepsilon_{18.7}/\Delta\varepsilon_{23.8}$ on 12 land surface types in USA; the abscissa values in the plots are day numbers in a year and the ordinate

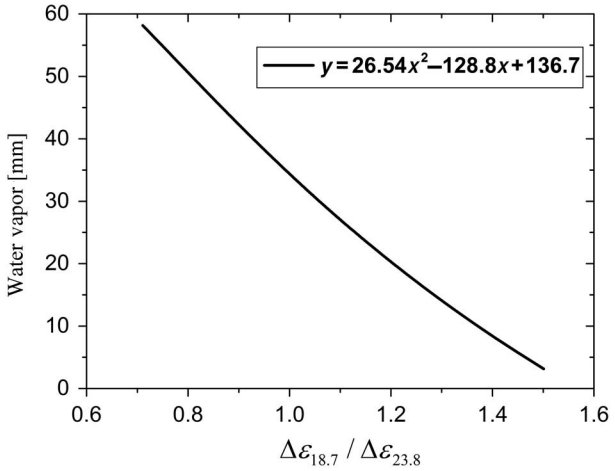

Fig. 3. Sensitivity of water vapor to $\Delta\varepsilon_{18.7}/\Delta\varepsilon_{23.8}$ with surface temperature = 300 K and $\Delta\mathrm{Tb}_{18.7}/\Delta\mathrm{Tb}_{23.8} = 1.6$.

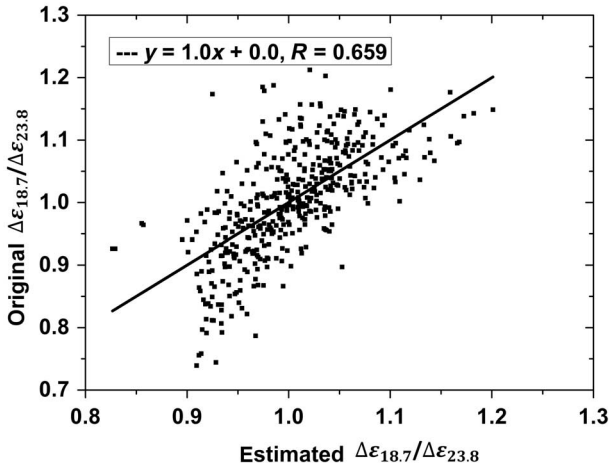

Fig. 4. Scatter diagram of estimated and real $\Delta\varepsilon_{18.7}/\Delta\varepsilon_{23.8}$ in clear condition. The solid line is diagonal.

values are $\Delta\varepsilon_{18.7}/\Delta\varepsilon_{23.8}$. According to these plots, the value of $\Delta\varepsilon_{18.7}/\Delta\varepsilon_{23.8}$ has a significant change over seasons on some kinds of land surface type, such as evergreen needle leaf forest, open shrub lands, woody savannas, grasslands, and croplands. While the value does not have significant seasonal change on some other kinds of land surface type, such as, evergreen broadleaf forest, mixed forest, permanent wetlands, and urban and build-up area. From the view of average value of $\Delta\varepsilon_{18.7}/\Delta\varepsilon_{23.8}$ at different surface types, $\Delta\varepsilon_{18.7}/\Delta\varepsilon_{23.8}$ is usually greater than 1 in the region of open shrublands, grasslands, and barren or sparsely vegetated areas. The reason for this phenomenon is that the land surface structure is relatively simple or "smooth," and the brightness temperature polarization difference decreases with increasing frequency at these land surface types. On the contrary, $\Delta\varepsilon_{18.7}/\Delta\varepsilon_{23.8}$ is usually smaller than 1 in the regions such as evergreen needle-leaf forest, evergreen broadleaf forest, and deciduous broadleaf forest. The structure of these land surfaces is very complex due to the existence of trees or buildings. It obscures the signal of lower bare surface transferring directly to the space-based radiometer and the frequency dependence of polarization difference is weakened. The theory about how the signal is affected by trees and building is outside the scope of this study, and it needs to be further studied in the future.

As shown in Fig. 2, $\Delta\varepsilon_{18.7}/\Delta\varepsilon_{23.8}$ has significant change over seasons and different surface types. The problem is that how much will $\Delta\varepsilon_{18.7}/\Delta\varepsilon_{23.8}$ affect the precision of the retrieved atmospheric water vapor. A simulation was performed using 1-DMWRTM and the outcome is shown in Fig. 3. This figure shows the sensitivity of water vapor to $\Delta\varepsilon_{18.7}/\Delta\varepsilon_{23.8}$ at a given surface temperature and $\Delta\mathrm{Tb}_{18.7}/\Delta\mathrm{Tb}_{23.8}$; according to this figure, the retrieved water vapor decreases with the increasing $\Delta\varepsilon_{18.7}/\Delta\varepsilon_{23.8}$, an error of 0.1 of $\Delta\varepsilon_{18.7}/\Delta\varepsilon_{23.8}$ may cause an average error of 7 mm of retrieved water vapor. As the valid range of $\Delta\varepsilon_{18.7}/\Delta\varepsilon_{23.8}$ is between 0.6 and 1.5 according to statistics, if $\Delta\varepsilon_{18.7}/\Delta\varepsilon_{23.8}$ is set to a constant in the retrieval of water vapor, it may result in significant error. So, it is necessary to estimate $\Delta\varepsilon_{18.7}/\Delta\varepsilon_{23.8}$ on a pixel-by-pixel basis.

It is easy to estimate $\Delta\varepsilon_{18.7}/\Delta\varepsilon_{23.8}$ in clear condition; however, it is difficult in cloudy condition due to lacking information of atmosphere. New method of estimating $\Delta\varepsilon_{18.7}/\Delta\varepsilon_{23.8}$ should be proposed to fulfill the need of water vapor retrieval. According to the analysis of relationship between $\Delta\varepsilon_{18.7}/\Delta\varepsilon_{23.8}$ and bands combination of AMSR-E in clear condition, it was found that $\Delta\varepsilon_{18.7}/\Delta\varepsilon_{23.8}$ can be expressed using a multiple linear regression equation

$$\Delta\varepsilon_{18.7}/\Delta\varepsilon_{23.8} = a * r6 + b * r10 + c * r18 + d * r36 + e * \mathrm{mvi\_l} \quad (5)$$

where a, b, c, d, and e are regression coefficients. $r6$, $r10$, $r18$, and $r36$ are ratios of vertical and horizontal polarimetric brightness temperatures at frequencies 6.925, 10.65, 18.7, and 36.5 GHz, respectively. $\mathrm{mvi\_l}$ is microwave vegetation index [29] at low frequencies (6.925 and 10.65 GHz). As a verification of (5), a random research area with $27 * 17$ pixels in clear condition is selected, and coefficients a, b, c, d, and e are estimated using multiple linear regression method with datasets including original $\Delta\varepsilon_{18.7}/\Delta\varepsilon_{23.8}$ (estimated using lookup table method mentioned above), $r6$, $r10$, $r18$, $r36$, and $\mathrm{mvi\_l}$ from the selected area. With these coefficients, a new estimated $\Delta\varepsilon_{18.7}/\Delta\varepsilon_{23.8}$ in clear condition can be calculated using (5). Fig. 4 shows scatter plot of the estimated $\Delta\varepsilon_{18.7}/\Delta\varepsilon_{23.8}$ and original $\Delta\varepsilon_{18.7}/\Delta\varepsilon_{23.8}$. The correlation coefficient of the two is about 0.66. Although the correlation coefficient is not very high, it indicates that (5) can be used to do an initial estimate of real $\Delta\varepsilon_{18.7}/\Delta\varepsilon_{23.8}$, and the initial estimate of $\Delta\varepsilon_{18.7}/\Delta\varepsilon_{23.8}$ will be further improved by new method introduced in the following part of this section.

For the original $\Delta\varepsilon_{18.7}/\Delta\varepsilon_{23.8}$ in clear condition, the value in each pixel is divided by mean value of its surrounding 15×15 pixels. This process can greatly remove the effect of atmosphere and enhance the information of land surface. The same processing method is applied to $\Delta\mathrm{Tb}_{18.7}/\Delta\mathrm{Tb}_{23.8}$, which is corresponding to the original $\Delta\varepsilon_{18.7}/\Delta\varepsilon_{23.8}$. The processed $\Delta\varepsilon_{18.7}/\Delta\varepsilon_{23.8}$ and $\Delta\mathrm{Tb}_{18.7}/\Delta\mathrm{Tb}_{23.8}$ are named as "adjusted $\Delta\varepsilon_{18.7}/\Delta\varepsilon_{23.8}$" and "adjusted $\Delta\mathrm{Tb}_{18.7}/\Delta\mathrm{Tb}_{23.8}$" for convenience. Fig. 5 shows scatter plot of the two adjusted datasets. This figure shows that the two datasets have very good linear

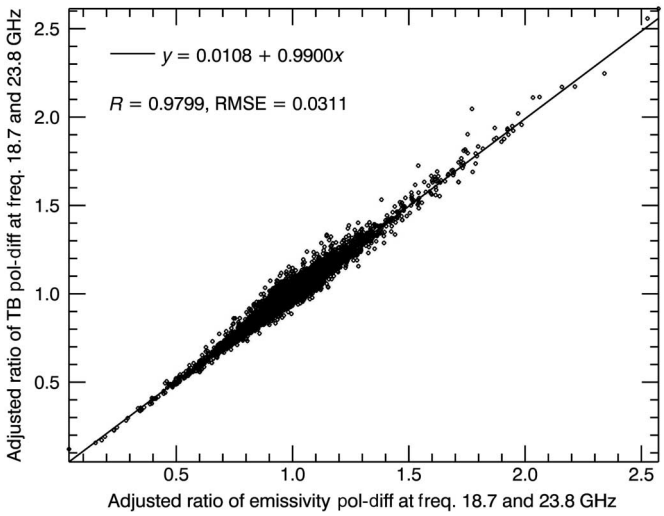

Fig. 5. Scatter diagram of adjusted $\Delta\varepsilon_{18.7}/\Delta\varepsilon_{23.8}$ and $\Delta\mathrm{Tb}_{18.7}/\Delta\mathrm{Tb}_{23.8}$.

correlation. The correlation coefficient of the two is 0.9799. Root-mean-square-error (RMSE) is 0.0311. The slope and intercept of the regression function are 0.99 and 0.0108, respectively. Good correlation of the two adjusted datasets provides a new method to improve the estimation of $\Delta\varepsilon_{18.7}/\Delta\varepsilon_{23.8}$. Equation (6) shows a method to improve the estimation of $\Delta\varepsilon_{18.7}/\Delta\varepsilon_{23.8}$ based on the outcome of (5)

$$\frac{(\Delta\varepsilon_{18.7}/\Delta\varepsilon_{23.8})_{(c,r)}}{(\Delta\varepsilon_{18.7}/\Delta\varepsilon_{23.8})_{\mathrm{mean}}^{15\times15}}=\frac{(\Delta\mathrm{Tb}_{18.7}/\Delta\mathrm{Tb}_{23.8})_{(c,r)}}{(\Delta\mathrm{Tb}_{18.7}/\Delta\mathrm{Tb}_{23.8})_{\mathrm{mean}}^{15\times15}} \quad (6)$$

where $(\Delta\varepsilon_{18.7}/\Delta\varepsilon_{23.8})_{(c,r)}$ is the value to be estimated, c and r are column and row number of the pixel in the image. $(\Delta\varepsilon_{18.7}/\Delta\varepsilon_{23.8})_{\mathrm{mean}}^{15\times15}$ is a mean value of 15×15 $\Delta\varepsilon_{18.7}/\Delta\varepsilon_{23.8}$ pixels grid whose center is the pixel that locates at positions c and r. $(\Delta\mathrm{Tb}_{18.7}/\Delta\mathrm{Tb}_{23.8})_{(c,r)}$ is $\Delta\mathrm{Tb}_{18.7}/\Delta\mathrm{Tb}_{23.8}$ that locates at positions c and r. $(\Delta\mathrm{Tb}_{18.7}/\Delta\mathrm{Tb}_{23.8})_{\mathrm{mean}}^{15\times15}$ is a mean value of 15×15 $\Delta\mathrm{Tb}_{18.7}/\Delta\mathrm{Tb}_{23.8}$ pixel grid whose center is the pixel that locates at positions c and r.

In cloudy condition, the initial estimate of $\Delta\varepsilon_{18.7}/\Delta\varepsilon_{23.8}$ is also calculated using (5) on a pixel-by-pixel basis. For a pixel in cloudy condition, coefficients in (5) should be first calculated before estimating $\Delta\varepsilon_{18.7}/\Delta\varepsilon_{23.8}$. The method to select datasets to calculate coefficients in (5) is shown in Fig. 6. In this figure, $\Delta\varepsilon_{18.7}/\Delta\varepsilon_{23.8}$ of red point locating at center of 15×15 grid in Day N is the point that will be estimated using (5). The datasets including $\Delta\varepsilon_{18.7}/\Delta\varepsilon_{23.8}$, $r6$, $r10$, $r18$, $r36$, and $\mathrm{mvi\_1}$ in clear condition locating at the 15×15 grids from Day $N-3$ to Day $N+4$ are selected to calculate coefficient in (5) using multiple linear regression method. With the calculated coefficients, $\Delta\varepsilon_{18.7}/\Delta\varepsilon_{23.8}$ at the red point in Day N can be estimated using the corresponding $r6$, $r10$, $r18$, $r36$, and $\mathrm{mvi\_1}$ in Day N. The $\Delta\varepsilon_{18.7}/\Delta\varepsilon_{23.8}$ of all pixels in cloudy condition can be estimated pixel by pixel using the same method. However, it is not accurate enough to retrieve water vapor using the estimated $\Delta\varepsilon_{18.7}/\Delta\varepsilon_{23.8}$ from (5). As an improvement, (6) is used to further improve the estimated $\Delta\varepsilon_{18.7}/\Delta\varepsilon_{23.8}$.

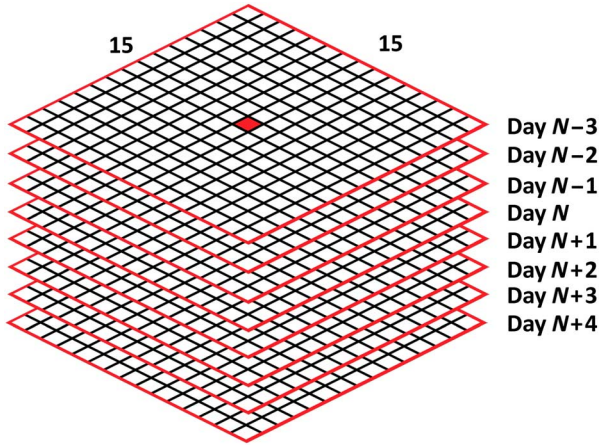

Fig. 6. Data selected to calculate coefficients in (5).

With the method mentioned above, the surface emissivity parameter $\Delta\varepsilon_{18.7}/\Delta\varepsilon_{23.8}$ in cloudy condition can be estimated precisely enough to be used in the retrieval of atmospheric water vapor. Although the $\Delta\varepsilon_{18.7}/\Delta\varepsilon_{23.8}$ in cloudy condition is not as precise as it is in clear condition, it provides a new way to estimate and optimize the estimation of $\Delta\varepsilon_{18.7}/\Delta\varepsilon_{23.8}$.

C. Cloud Effect Analysis

Existence of clouds brings great difficulty to the retrieval of atmospheric water vapor. On the one hand, clouds existence obstacles signals emitted from surface transferred to satellite and makes it difficult to estimate surface boundary parameters under cloud. This problem is solved to a certain extent in Section IV in the retrieval of atmospheric water vapor in this study. On the other hand, signals attenuated or emitted by clouds will contribute to the signal of water vapor. Although water vapor sensitive bands combination ($\Delta\mathrm{Tb}_{18.7}/\Delta\mathrm{Tb}_{23.8}$) is selected to suppress the effect of cloud in the retrieval of atmospheric water vapor, it is not possible to eliminate the effect of cloud completely. As the absorption coefficient of a cloud is simply proportional to the mass density of the water contained in the cloud independent of the details of the size distribution of the droplets as long as all the particles are much smaller than the wavelength [30], the effect of clouds to $\Delta\mathrm{Tb}_{18.7}/\Delta\mathrm{Tb}_{23.8}$ is mainly contributed by cloud liquid water. Fig. 7 shows a simulation of 1-DMWRTM. In this figure, sensitivities of normalized ratio of $\Delta\mathrm{Tb}$ at two frequencies to cloud liquid water are represented in different line types. According to Fig. 7, $\Delta\mathrm{Tb}_{18.7}/\Delta\mathrm{Tb}_{23.8}$ has the least sensitivity to cloud liquid water compared with other frequencies combination, but there is still about 10% change in $\Delta\mathrm{Tb}_{18.7}/\Delta\mathrm{Tb}_{23.8}$, as the cloud liquid water increasing from 0 to 1 mm, and this change will finally affect the precision of retrieved water vapor. A quantitative analysis of cloud effects to $\Delta\mathrm{Tb}_{18.7}/\Delta\mathrm{Tb}_{23.8}$ is very necessary, as it may improve the accuracy of retrieved water vapor.

According to a simulation by 1-DMWRTM, the effect of cloud fraction and cloud liquid water to $\Delta\mathrm{Tb}_{18.7}/\Delta\mathrm{Tb}_{23.8}$ is analyzed and the simulation is shown in Fig. 8. This figure shows the effect of cloud to $\Delta\mathrm{Tb}_{18.7}/\Delta\mathrm{Tb}_{23.8}$, when $\Delta\varepsilon_{18.7}/\Delta\varepsilon_{23.8}=0.8$. In Fig. 8, the abscissa values are cloud fraction

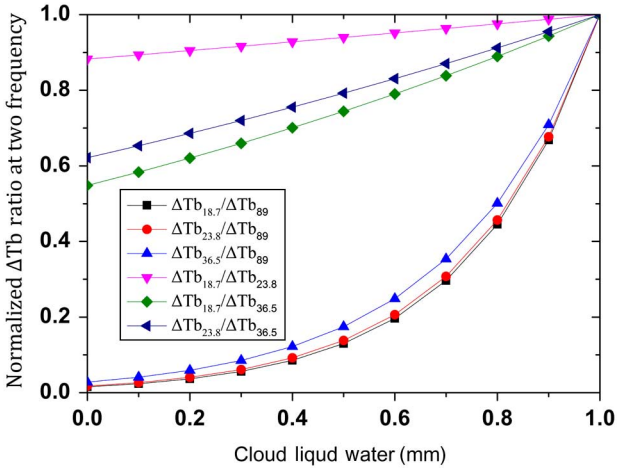

Fig. 7. Sensitivity of normalized ratio of $\Delta\mathrm{Tb}$ at two frequencies to cloud liquid water.

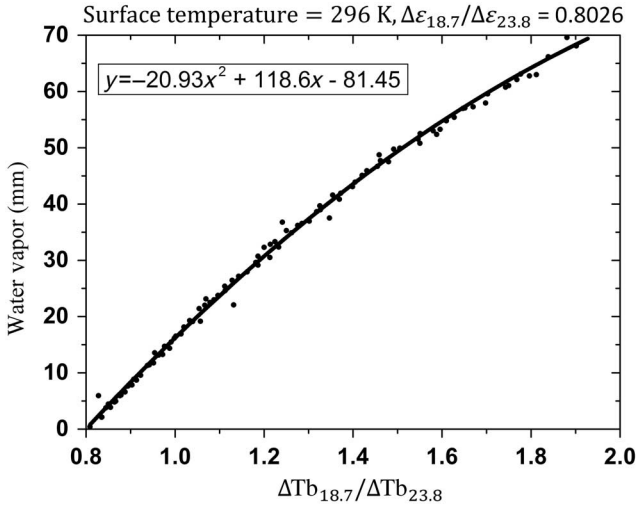

Fig. 9. Simulated sensitivity of water vapor to $\Delta\mathrm{Tb}_{18.7}/\Delta\mathrm{Tb}_{23.8}$ by 1-DMWRTM, when surface temperature is 296 K and $\Delta\varepsilon_{18.7}/\Delta\varepsilon_{23.8}$ is 0.8026.

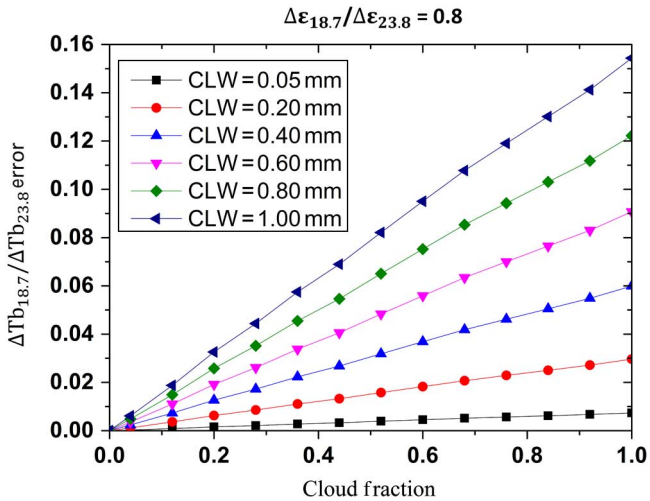

Fig. 8. Simulated error of $\Delta\mathrm{Tb}_{18.7}/\Delta\mathrm{Tb}_{23.8}$ caused by cloud using 1-DMWRTM, when $\Delta\varepsilon_{18.7}/\Delta\varepsilon_{23.8}$ is 0.8.

and the ordinate values are errors of $\Delta\mathrm{Tb}_{18.7}/\Delta\mathrm{Tb}_{23.8}$ caused by cloud and different line types in the plot denote different cloud liquid water. From Fig. 8, we can see that the error of $\Delta\mathrm{Tb}_{18.7}/\Delta\mathrm{Tb}_{23.8}$ increases with cloud fraction and cloud liquid water. When cloud fraction is equal to 1 and cloud liquid water is up to 1 mm, the maximum error of $\Delta\mathrm{Tb}_{18.7}/\Delta\mathrm{Tb}_{23.8}$ caused by cloud is about 0.16. While in natural state, it is rare that cloud liquid water reaches up to 1 mm. For example, for all liquid water path (LWP) retrievals based on a ground-based microwave radiometer at the ARM SGP site over an entire year (including both clear and cloudy conditions), retrieved LWP was less than 0.1 mm about 83% of the time, and about 12% of the LWP retrievals in the same dataset exceeded 0.2 mm [12]. Cloud liquid water of 0.1 and 0.2 mm will cause 0.016 and 0.03 changes in $\Delta\mathrm{Tb}_{18.7}/\Delta\mathrm{Tb}_{23.8}$, respectively. Fig. 9 shows sensitivity of water vapor to $\Delta\mathrm{Tb}_{18.7}/\Delta\mathrm{Tb}_{23.8}$, and the fitting equation of the two is $y = -20.93x^2 + 118.6x - 81.45$, where y is water vapor and x is $\Delta\mathrm{Tb}_{18.7}/\Delta\mathrm{Tb}_{23.8}$. We differentiate this equation with respect to x, and then we get equation $y' = dy/dx = -41.86x + 118.6$. From this equation, $\Delta\mathrm{Tb}_{18.7}/\Delta\mathrm{Tb}_{23.8}$ errors of 0.16, 0.03, and 0.016 corresponding to the retrieved water vapor errors are 12.3, 2.3, and 1.2 mm, respectively, at position $x = 1$. As the clouds with 1 mm of cloud liquid water seldom appear commonly, the error of retrieved water vapor caused by cloud is less than about 2.3 mm and 83% of the errors will be less than 1.2 mm. Although the error caused by cloud is very small compared with water vapor of the whole layer of atmosphere, it is necessary to do correction to remove the effect of thick cloud and to further improve the accuracy of water vapor. As a correction method for cloud effect, a lookup table method is used. The lookup table is built using 1-DMWRTM, and it includes four fields, $\Delta\varepsilon_{18.7}/\Delta\varepsilon_{23.8}$, cloud liquid water, cloud fraction in a pixel, and error of $\Delta\mathrm{Tb}_{18.7}/\Delta\mathrm{Tb}_{23.8}$. When applying correction, the value of $\Delta\varepsilon_{18.7}/\Delta\varepsilon_{23.8}$, cloud liquid water, and cloud fraction in a pixel are used as input parameters and then the error of $\mathrm{Tb}_{18.7}/\Delta\mathrm{Tb}_{23.8}$ is calculated using a lookup table searching method. Finally, the error of $\Delta\mathrm{Tb}_{18.7}/\Delta\mathrm{Tb}_{23.8}$ is subtracted from $\Delta\mathrm{Tb}_{18.7}/\Delta\mathrm{Tb}_{23.8}$ to get a corrected $\Delta\mathrm{Tb}_{18.7}/\Delta\mathrm{Tb}_{23.8}$. The value of $\Delta\varepsilon_{18.7}/\Delta\varepsilon_{23.8}$ is estimated using the method mentioned in Section III-B, and the value of cloud liquid water and cloud fraction is retrieved from MODIS cloud product (MYD06). However, due to the limitation of the algorithm of MODIS cloud product, only daytime cloud liquid water data are provided by MYD06. So, in this research, only daytime $\Delta\mathrm{Tb}_{18.7}/\Delta\mathrm{Tb}_{23.8}$ data are corrected in the water vapor retrieval.

D. Water Vapor Retrieval

In the retrieval of atmospheric water vapor, vertical distribution variation in water vapor profile will also affect brightness temperature at the top of atmosphere. The variation destroys monotonic changing property of $\Delta\mathrm{Tb}_{18.7}/\Delta\mathrm{Tb}_{23.8}$ as water vapor increases and will bring errors to the retrieval of water vapor. As a solution to reduce the errors, transmittances of water vapor at frequencies 18.7 and 23.8 GHz are used as

intermediate variables to retrieve water vapor. In the retrieval process, the transmittance of water vapor is first retrieved and then it is converted to water vapor. These transmittances are good indicators of water vapor, and at the same time, they can reduce errors caused by vertical variation in profiles to a certain extent by weighed averaging water vapor transmittances estimated at different frequencies.

Before we finally get the retrieved atmospheric water vapor, transmittances of water vapor at frequency 18.7 and 23.8 GHz are first estimated using the lookup table method. The lookup table is built based on the theories mentioned in Section III-A with the help of 1-DMWRTM, and it contains four fields: surface temperature, $\Delta\varepsilon_{18.7}/\Delta\varepsilon_{23.8}$, transmittance at a frequency, and $\Delta\mathrm{Tb}_{18.7}/\Delta\mathrm{Tb}_{23.8}$. There are two frequencies (18.7 and 23.8 GHz), so two lookup table of this kind will be built. In order to convert transmittance at different frequencies to water vapor, another lookup table is build using atmospheric profiles from radiosonde observations and 1-DMWRTM. The lookup table contains column water vapor of the atmospheric profiles from radiosonde and its corresponding two transmittances of water vapor at frequency 18.7 and 23.8 GHz. Total error between the estimated transmittances at the two frequencies and that in the lookup table is calculated using (7).

$$t_{\mathrm{err}} = (t_{18.7}^{\mathrm{est}} - t_{18.7}^{\mathrm{lut}}) + (t_{23.8}^{\mathrm{est}} - t_{23.8}^{\mathrm{lut}}) \tag{7}$$

where t_{err} is the total error, $t_{18.7}^{\mathrm{est}}$ and $t_{23.8}^{\mathrm{est}}$ are transmittances estimated using the method mentioned in the last paragraph. $t_{18.7}^{\mathrm{lut}}$ and $t_{23.8}^{\mathrm{lut}}$ are transmittances derived from lookup table. Water vapor values corresponding to the 10 smallest t_{err} will be selected in the lookup table and then those water vapor values will be combined together to form the final retrieved column water vapor using (8)

$$\mathrm{CWV} = \sum\nolimits_{i=1}^{10} \mathrm{CWV}_i * W_i \tag{8}$$

where CWV is the final retrieved water vapor, $\mathrm{CWV_i}$ is one of water vapor selected from the lookup table, $\mathrm{W_i}$ is weight coefficient corresponding to $\mathrm{CWV_i}$, and it is calculated using (9)

$$W_i = \sum\nolimits_{j=1}^{10} t_{\mathrm{err}}^j - t_{\mathrm{err}}^i \Big/ \sum\nolimits_{i=1}^{10} \left(\sum\nolimits_{j=1}^{10} t_{\mathrm{err}}^j - t_{\mathrm{err}}^i \right). \tag{9}$$

In (9), the $\sum_{j=1}^{10} t_{\mathrm{err}}^j$ must be lower than 0.05, if not, the column water vapor on the corresponding pixel will be set to invalid.

The following is a general description of atmospheric water vapor retrieval algorithm. Fig. 10 shows the flowchart of water vapor retrieval algorithm. Data used in the algorithm include AMSR-E brightness temperature, MODIS products, and radiosonde observations. AMSR-E brightness temperature and MODIS product are mainly used to estimate surface parameters and column water vapor. Radiosonde observations are mainly used to build lookup table.

As shown in Fig. 10, all the related AMSR-E and MODIS products are re-projected into $0.25^\circ \times 0.25^\circ$ grid images. The land sea mask derived from AMSR-E and cloud mask from MODIS cloud mask product are used to constraint the algorithm only running under cloud cover area on land. As our algorithm is not suitable for rainy condition, the rainy pixels are detected and removed using method mentioned in [31]. Then $\Delta\mathrm{Tb}_{18.7}/\Delta\mathrm{Tb}_{23.8}$ is calculated using the re-projected AMSR-E brightness temperature, and it is corrected with cloud liquid water information of MODIS cloud product. Before water vapor transmittance is estimated, we still need more information that includes surface temperature estimated from AMSR-E and MODIS product, surface emissivity parameter $\Delta\varepsilon_{18.7}/\Delta\varepsilon_{23.8}$ estimated by the method mentioned in Section III-B, and a lookup table. The lookup table is built to estimate water vapor transmittances at frequencies 18.7 and 23.8 GHz using 1-DMWRTM and atmospheric profiles from radiosonde observations based on the theory mentioned in Section III-A. Four fields are included in the lookup table; they are surface temperature, $\Delta\varepsilon_{18.7}/\Delta\varepsilon_{23.8}$, water vapor transmittance at its corresponding frequency, and $\Delta\mathrm{Tb}_{18.7}/\Delta\mathrm{Tb}_{23.8}$. With this information, the water vapor transmittance at 18.7 and 23.8 GHz can then be estimated. In order to convert water vapor transmittance to water vapor content, another lookup table is build using the atmospheric profiles from radiosonde observations. The lookup table contains water vapor content of atmospheric profiles from radiosonde observations and their corresponding water vapor transmittance at two frequencies, 18.7 and 23.8 GHz. At last, with this converting lookup table, the water vapor is retrieved.

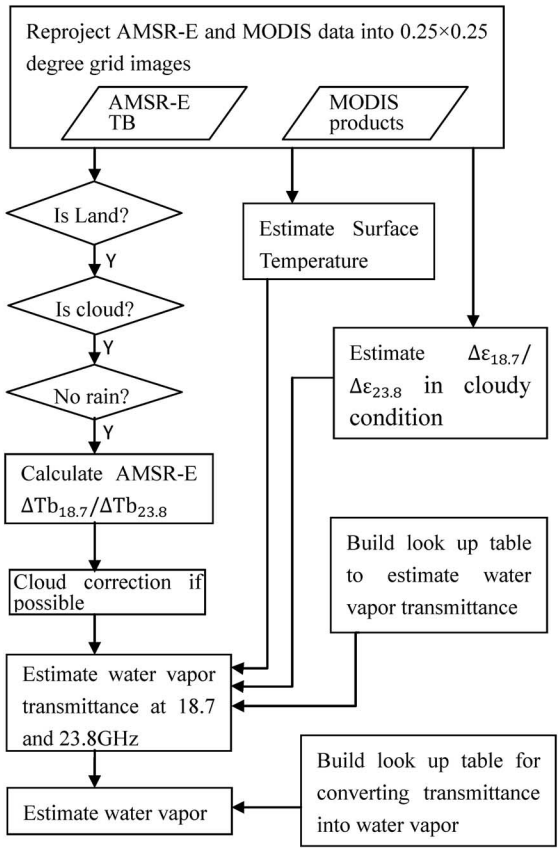

Fig. 10. Flowchart of water vapor retrieval in this study.

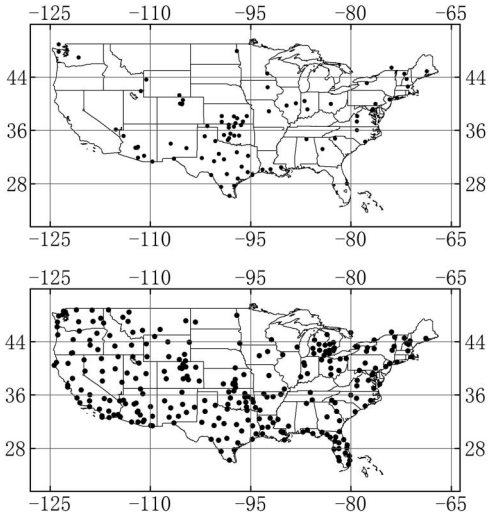

Fig. 11. SuomiNet GPS sites distribution map in USA, the upper figure is available GPS sites in January 2007; the bottom figure is available GPS sites in July 2007.

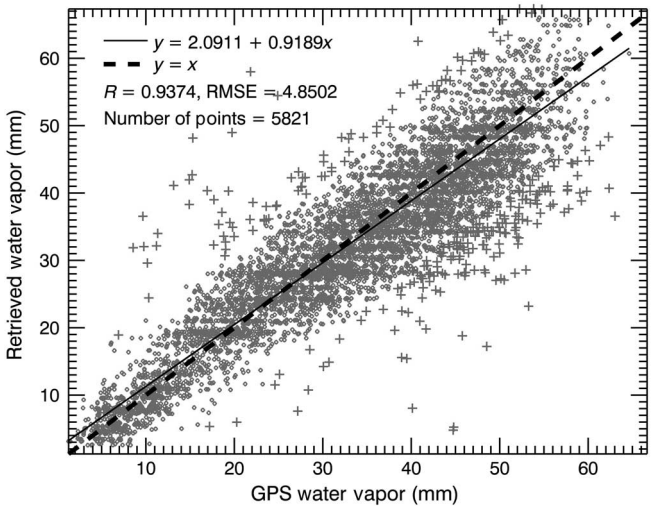

Fig. 12. Scatter diagram of retrieved water vapor versus GPS water vapor, January and July 2007. The dashed line is diagonal and the solid line is regression line of the two comparison datasets.

IV. Validation and Error Analysis

A. Comparison With GPS Observation

The SuomiNet GPS retrieved PW vapor is used as the source of validation data. Each of these sites provides an observation of PW vapor every half hour. When using the GPS water vapor for validation of AMSR-E, it is possible to account for the different spatial scales of the two sensors by time averaging the GPS observation [32]. In this study, an hourly averaged GPS-retrieved PW vapor is used to validate column water vapor retrieved from AMSR-E. In the validation, all the GPS sites observation data from January 1, 2007 to January 31, 2007 and July 1, 2007 to July 31, 2007 located in USA over cloud cover area on land are used as validation data. Fig. 11 shows the SuomiNet GPS sites distribution map in USA. The upper figure shows available GPS sites during January 2007 and the bottom figure shows available GPS sites during July 2007.

In order to validate the effect of cloud correction in water vapor retrieval, two categories of water vapor are retrieved. One category of water vapor is retrieved using original $\Delta\mathrm{Tb}_{18.7}/\Delta\mathrm{Tb}_{23.8}$. The other is retrieved using $\Delta\mathrm{Tb}_{18.7}/\Delta\mathrm{Tb}_{23.8}$, which is corrected using cloud liquid water information from MODIS. The scatter plots of retrieved water vapor without considering cloud effect versus the GPS retrieved water vapor are shown in Fig. 12. This figure shows the comparison using data from January to July 2007. According to the validation method by [13] and [32], the worst 5% match-up data are removed from both sides of regression line and the removed match-up data are also plotted in the figure with symbol "+". This reduces the effects of poor quality match-up data on the validation. There are two reasons for the removing of worst match-up data. One of them is that the spatial and temporal difference between observation of satellite and GPS. The other is that none-detected drizzle and light precipitation will impact the measurement of microwave signal, which will result in an underestimation of atmospheric water vapor [13]. With the datasets after removing the worst match-up data, a statistic of the comparison is shown in Fig. 12.

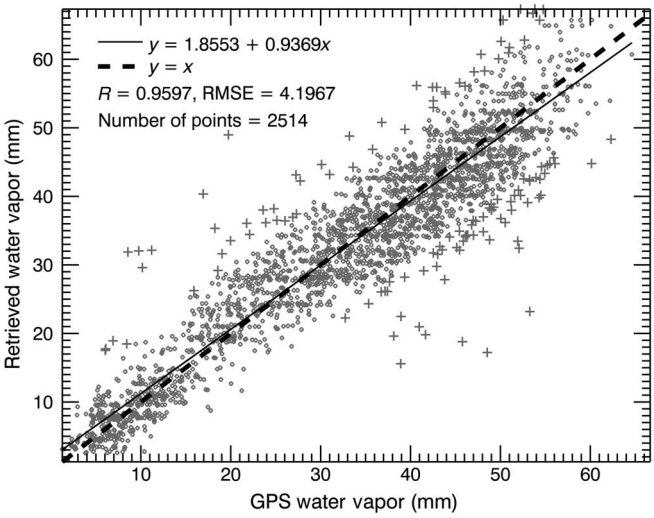

Fig. 13. Scatter plot of retrieved water vapor in ascending orbit without cloud liquid water correction versus GPS retrieved water vapor, January and July 2007. The dashed line is diagonal and the solid line is regression line of the two comparison datasets.

In Fig. 12, the thick dashed line is the diagonal. The thin solid line is the regression line of the two datasets. The slope and the intercept of the regression line are 0.92 and 2.09 mm, respectively. The correlation coefficient is 0.94 and the RMSE is 4.85 mm. The lower value of slope indicates an underestimation at high atmospheric water vapor, which may attribute to an increment of undetected light precipitation in summer season.

As MODIS onboard AQUA only providing cloud liquid water information in daytime, the retrieved two water vapor categories in ascending orbit are used in the comparison. Fig. 13 shows scatter plot of retrieved column water vapor in ascending orbit without cloud liquid water correction versus GPS-retrieved PW vapor in January and July 2007. Fig. 14 shows same scatter plot, but the retrieved column water vapor is corrected using cloud

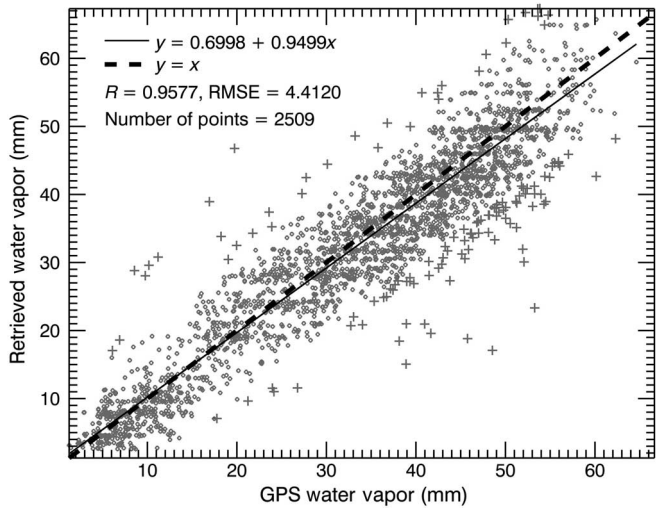

Fig. 14. Scatter plot of retrieved water vapor in ascending orbit with cloud liquid water correction versus GPS retrieved water vapor, January and July 2007. The dashed line is diagonal and the solid line is regression line of the two comparison datasets.

liquid water information from MODIS. In Fig. 13, the slope and intercept of the regression line are 0.94 and 1.86, respectively, the correlation coefficient is 0.96, and the RMSE is 4.19 mm. In Fig. 14, the corresponding four parameters are 0.95, 0.70, 0.96, and 4.41 mm, respectively. According to the comparison of the two scatter plots, a correction of cloud liquid water effect to the retrieved water vapor improves the intercept of regression equation from 1.86 to 0.70 and slope of regression equation from 0.94 to 0.95. However, the correction of cloud does not bring any improvement to correlation coefficient and RMSE. There are many reasons for such little improvement. The most important one is that 83% errors caused by cloud is less than 1.2 mm as mentioned above, this error estimation is based on that the cloud liquid water is correctly known. However, on satellite Aqua, the currently available cloud liquid water over land is only provided by MODIS. The cloud liquid water from MODIS is retrieved only according to cloud top information. It will bring great errors in situation of thick clouds or multi-layer clouds. Another reason may attribute to data and model used in the correction of cloud effect. It is difficult for the model 1-DMWRTM to simulate microwave radiative transfer process in cloud precisely, as the complexity, quick change of clouds, and limited understanding coupling effect of water vapor and cloud liquid water in radiative transfer process. These above-mentioned reasons affect the correction of cloud liquid water on the retrieval of atmospheric water vapor. The theory of the coupling effect of water vapor and cloud and the retrieval of cloud liquid water over land are beyond the scope of this study. It needs further study in future about these problems.

B. Map of Atmospheric Water Vapor Distribution

Currently, there is no passive microwave radiometer such as TRMM-TMI and AMSR-E providing available water vapor dataset over land. Satellite-based infrared water vapor retrievals are also limited by clouds. Lack of precise water vapor over land may bring limitation to the research of climate system and hydrological cycle. The algorithm in this study provides a new

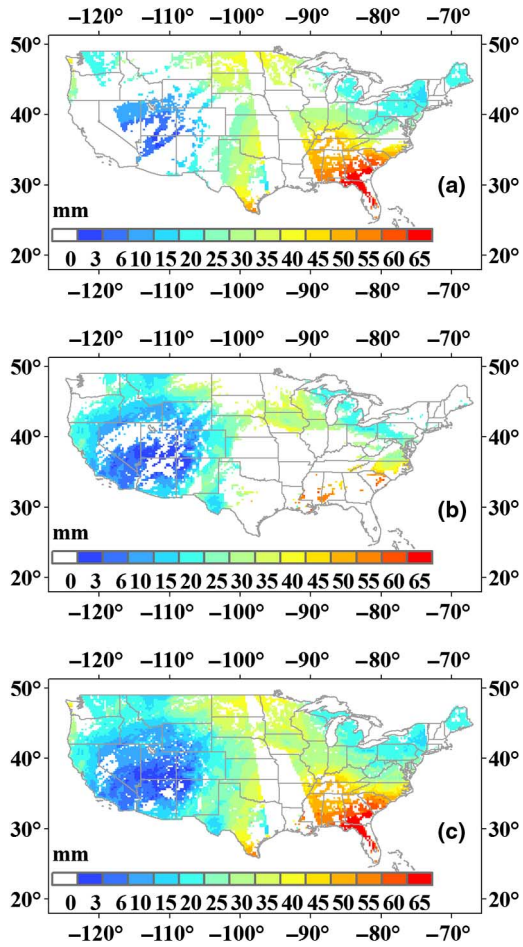

Fig. 15. Atmospheric water vapor distribution map of USA on July 1, 2007, ascending orbit: (a) the distribution of atmospheric water vapor retrieved by AMSR-E under cloudy condition, (b) the distribution of atmospheric water vapor in clear condition from MODIS water vapor product, and (c) a combination of atmospheric water vapor distribution from (a) and (b).

solution to retrieve atmospheric water vapor over land on cloudy condition, which makes it possible to create a complete atmospheric water vapor map over land for every swath of satellite observation combined with water vapor data retrieved from MODIS in clear condition. For view of water vapor distribution in spatial scale, Fig. 15 shows water vapor distribution map of U.S. mainland derived from Aqua satellite in ascending orbit on July 1, 2007. Fig. 15(a) shows a map of atmospheric water vapor in cloudy condition retrieved using algorithm in this study based on the data of AMSR-E; Fig. 15(b) shows an atmospheric water vapor data from MODIS onboard Aqua satellite, and Fig. 15(c) is a combination of Fig. 15(a) and (b), as it shows a complete atmospheric water map over U.S. mainland except the area with precipitation or that lack of observation. From the map of atmospheric water vapor, it shows obvious regional distribution difference. Most of water vapor with the highest value reaching up to 65 mm distributes in south east part of U.S. mainland due to the Warm Current of Mexico Gulf that brings abundant water vapor to Florida and the surrounding area. Low water vapor (lower than 3 mm) occurs in the western inland area of America, which attribute to Rocky Mountain that blocks warm current coming from the Pacific.

C. Possible Error Sources in Retrieval

Although the error of retrieved atmospheric water vapor has improved a lot compared with former research, there are still some factors that are to be considered in actual retrieval. First of all, the accuracy of estimated surface emissivity parameter $\Delta\varepsilon_{18.7}/\Delta\varepsilon_{23.8}$ plays an important role to the precision of retrieved atmospheric water vapor. As signal from surface contributes most part of signal received by satellite, a small change in surface condition will bring great uncertainty to the retrieved water vapor. However, a new method had been put forward in this study to estimate the surface emissivity parameter $\Delta\varepsilon_{18.7}/\Delta\varepsilon_{23.8}$ with the combination of AMSR-E brightness temperature and MODIS atmospheric products. Although the method cannot eliminate the error caused by uncertainty of surface emissivity, it reduces the error of retrieved atmospheric water vapor to acceptable levels over land. Cloud existence is another factor that affects retrieval of water vapor. On one hand, it affects estimation of surface emissivity parameter. On the other hand, signal from water vapor is contaminated by scatter, absorption of cloud, and signal emitted from cloud. It is difficult to entirely distinguish cloud information from water vapor. As a solution, the bands combination $\Delta\mathrm{Tb}_{18.7}/\Delta\mathrm{Tb}_{23.8}$ can effectively suppress signal of cloud from water vapor. It can reduce 83% errors caused by cloud to less than 1.2 mm. The errors caused by cloud can be further reduced, if cloud liquid water information is provided. However, it is also difficult to retrieve cloud liquid water over land. It will need further research to solve this problem in the future. The third error source is the uncertainty of surface temperature. The error of the estimated surface temperature is 4.5 K [28]; the impact of uncertainty of surface temperature can be ignored when the water vapor is small in atmosphere, but it increases as water vapor getting larger in atmosphere, typically in summer. Furthermore, light precipitation may not be effectively detected. The light precipitation can scatter and absorb the signal emitted from surface or water vapor of lower atmosphere and place an impact on the brightness temperature of radiometer, which result in an underestimated of atmospheric water vapor [13]. Finally, the error caused by the model 1-DMWRTM should not be ignored.

V. Conclusion

In this study, a newly developed algorithm is used to retrieve atmospheric water vapor in cloudy condition without precipitation over land based on the measurement of AMSR-E and MODIS. A water vapor sensitivity parameter $\Delta\mathrm{Tb}_{18.7}/\Delta\mathrm{Tb}_{23.8}$ defined in [12] is used in the retrieval with the help of a newly developed surface emissivity parameter estimation method.

An advantage of this algorithm is the estimation of surface emissivity parameter $\Delta\varepsilon_{18.7}/\Delta\varepsilon_{23.8}$ in cloudy condition over land using the measurement of AMSR-E combined with MODIS. As the signal received by passive microwave radiometer is a combination signal of ground surface and atmosphere, it is of vital importance to precisely estimate $\Delta\varepsilon_{18.7}/\Delta\varepsilon_{23.8}$. Compared to algorithms that ignore or set surface emissivity to a constant, the estimation of surface emissivity can effectively reduce errors caused by variation of surface condition in spatial and temporal scale, especially over land.

Cloud is the biggest obstacle in the retrieval of water vapor in cloudy condition. It not only brings difficulty to directly estimation of the surface emissivity parameter $\Delta\varepsilon_{18.7}/\Delta\varepsilon_{23.8}$ but also contaminates signal of water vapor received by satellite. For the first problem, the $\Delta\varepsilon_{18.7}/\Delta\varepsilon_{23.8}$ in cloudy condition can be estimated according to (5) and (6). For the second problem, the combination of bands $\Delta\mathrm{Tb}_{18.7}/\Delta\mathrm{Tb}_{23.8}$ can greatly enhance the information of water vapor and suppress the signal of cloud. Although $\Delta\mathrm{Tb}_{18.7}/\Delta\mathrm{Tb}_{23.8}$ cannot entirely remove the effect of cloud, it is able to reduce 83% errors caused by clouds to less than 1.2 mm. As a further step to remove the effect of cloud, cloud liquid water and cloud fraction information from MODIS are used in retrieval of water vapor. However, it only brings little improvement to the retrieved water vapor, which may attribute to the cloud liquid water provided by MODIS being not accurate enough. It needs further research in the future to separate cloud from water vapor signal.

The column water vapor was retrieved in cloudy condition over U.S. mainland in January and July of 2007. It was compared with GPS retrieved water vapor. According to the comparison, the RMSE-retrieved atmospheric water vapor in this study is 4.85 mm. The precision is acceptable for passive microwave remote sensing of atmospheric water vapor over land compared with the retrieved water vapor with RMSE of 6 mm over land in [12] and RMSE of 4.9 mm in cloudy condition over land in [17].

The algorithm for retrieval of water vapor using passive microwave remote sensing in cloudy condition over land is a complement to current water vapor retrieval algorithm. It can be used to produce a full cover water vapor map on each swath of observation combined with MODIS water vapor product. The algorithm is also suitable for other microwave radiometer such as TRMM-TMI or the newly launched AMSR2 with the help of geostationary satellite, and it will provide more valuable information for the research of climate change and hydrologic cycle.

Acknowledgments

The authors greatly appreciate the anonymous reviewers for their valuable comments. AMSR-E brightness temperature datasets were obtained from NASA's Earth Observing System Data Information System at http://reverb.echo.nasa.gov/reverb/. MODIS atmospheric products were obtained from NASA's Goddard Space Flight Center at http://ladsweb.nascom.nasa.gov/data/. The radiosonde atmospheric profile datasets were proved by Mr. Wang Yongqian at Chengdu University of Information Technology. SuomiNet datasets were obtained from http://www.suominet.ucar.edu/index.html.

References

[1] AGU, WATER VAPOR in the CLIMATE SYSTEM Special Report, Dec. 1995 [Online]. Available: http://www.eso.org/gen-fac/pubs/astclim/espas/pwv/mockler.html.

[2] Y. J. Kaufman and B. C. Gao, "Remote sensing of water vapor in the near IR from EOS/MODIS," *IEEE Trans. Geosci. Remote Sens.*, vol. 30, no. 5, pp. 871–884, Sep. 1992.

[3] B. C. Gao and Y. J. Kaufman, "Water vapor retrievals using Moderate Resolution Imaging Spectroradiometer (MODIS) near-infrared channels," *J. Geophys. Res.*, vol. 108, no. D13, p. 4389, Jul. 2003.
[4] T. Aoki and T. Inoue, "Estimation of the precipitable water from the IR channel of the geostationary satellite," *Remote Sens. Environ.*, vol. 12, no. 3, pp. 219–228, Jul. 1982.
[5] D. Chesters, W. D. Robinson, and L. W. Uccellini, "Optimized retrievals of precipitable water from the VAS 'split window'," *J. Clim. Appl. Meteor.*, vol. 26, no. 8, pp. 1059–1066, Aug. 1987.
[6] G. J. Jedlovec, "Precipitable water estimation from high-resolution split window radiance measurements," *J. Appl. Meteor.*, vol. 29, no. 9, pp. 863–877, Sep. 1990.
[7] A. R. Guillory, G. J. Jedlovec, and H. E. Fuelberg, "A technique for deriving column-integrated water content using VAS split-window data," *J. Appl. Meteor.*, vol. 32, no. 7, pp. 1226–1241, Jul. 1993.
[8] R. D. Knabb and H. E. Fuelberg, "A comparison of the first-guess dependence of precipitable water estimates from three techniques using GOES data," *J. Appl. Meteor.*, vol. 36, no. 5, pp. 417–427, May. 1997.
[9] N. C. Grody, "Remote sensing of atmospheric water content from satellites using microwave radiometry," *IEEE Trans. Antennas Propag.*, vol. 24, no. 2, pp. 155–162, Mar. 1976.
[10] N. C. Grody, A. Gruber, and W. C. Shen, "Atmospheric water content over the tropical pacific derived from the nimbus-6 scanning microwave spectrometer," *J. Appl. Meteor.*, vol. 19, no. 8, pp. 986–996, Aug. 1980.
[11] J. C. Alishouse, S. A. Snyder, J. Vongsathorn, and R. R. Ferraro, "Determination of oceanic total precipitable water from the SSM/I," *IEEE Trans. Geosci. Remote Sens.*, vol. 28, no. 5, pp. 811–816, Sep. 1990.
[12] M. N. Deeter, "A new satellite retrieval method for precipitable water vapor over land and ocean," *Geophys. Res. Lett.*, vol. 34, no. 2, p. L02815, Jan. 2007.
[13] Y. Wang, Y. Fu, G. Liu, Q. Liu, and L. Sun, "A new water vapor algorithm for TRMM Microwave Imager (TMI) measurements based on a log linear relationship," *J. Geophys. Res.*, vol. 114, no. D21, p. D21304, Nov. 2009.
[14] Y. Q. Wang, *The Study of Algorithms for Retrieving Atmospheric Parameters by Passive Microwave Remote Sensing and Atmospheric Correction for Passive Microwave Remote Sensing*, Beijing, China: Chinese Academy of Science, 2010.
[15] S. A. Tjemkes, G. L. Stephens, and D. L. Jackson, "Spaceborne observation of columnar water vapor: SSMI observations and algorithm," *J. Geophys. Res.*, vol. 96, no. D6, pp. 10941–10954, Jun. 1991.
[16] F. J. Wentz, "A well-calibrated ocean algorithm for special sensor microwave/imager," *J. Geophys. Res.*, vol. 102, no. C4, pp. 8703–8718, Apr. 1997.
[17] F. Aires, C. Prigent, W. B. Rossow, and M. Rothstein, "A new neural network approach including first guess for retrieval of atmospheric water vapor, cloud liquid water path, surface temperature, and emissivities over land from satellite microwave observations," *J. Geophys. Res.*, vol. 106, no. D14, pp. 14887–14907, Jul. 2001.
[18] L. P. Bobylev, E. V. Zabolotskikh, L. M. Mitnik, and M. L. Mitnik, "Atmospheric water vapor and cloud liquid water retrieval over the arctic ocean using satellite passive microwave sensing," *IEEE Trans. Geosci. Remote Sens.*, vol. 48, no. 1, pp. 283–294, Jan. 2010.
[19] A. S. Jones and T. H. Vonder Haar, "Passive microwave remote sensing of cloud liquid water over land regions," *J. Geophys. Res.*, vol. 95, no. D10, pp. 16673–16683, Sep. 1990.
[20] T. J. Greenwald, C. L. Combs, A. S. Jones, D. L. Randel, and T. H. Vonder Haar, "Further developments in estimating cloud liquid water over land using microwave and infrared satellite measurements," *J. Appl. Meteor.*, vol. 36, no. 4, pp. 389–405, Apr. 1997.
[21] W. S. Olson, P. Bauer, N. F. Viltard, D. E. Johnson, W. K. Tao, R. Meneghini, and L. Liao, "A melting-layer model for passive/active microwave remote sensing applications. Part I: Model formulation and comparison with observations," *J. Appl. Meteor.*, vol. 40, no. 7, pp. 1145–1163, Jul. 2001.
[22] W. S. Olson, P. Bauer, C. D. Kummerow, Y. Hong, and W. K. Tao, "A melting-layer model for passive/active microwave remote sensing applications. Part II: Simulation of TRMM observations," *J. Appl. Meteor.*, vol. 40, no. 7, pp. 1164–1179, Jul. 2001.
[23] R. H. Ware, D. W. Fulker, S. A. Stein, D. N. Anderson, S. K. Avery, R. D. Clark, K. Droegemeier, J. P. Kuettner, and J. B. Minster, "Suominet: A real-time national GPS network for atmospheric research and education," *Bull. Amer. Meteorol. Soc.*, vol. 81, no. 4, pp. 677–694, Apr. 2000.
[24] JAXA, *AMSR-E Data Users Handbook*, 4th ed., Saitama, Japan: JAXA Earth Observation Center, 2006. [Online]. Available: Available: http://www.eorc.jaxa.jp/en/hatoyama/amsr-e/amsr-e_handbook_e.pdf.
[25] M. Bevis, S. Businger, T. A. Herring, C. Rocken, R. A. Anthes, and R. H. Ware, "GPS meteorology: Remote sensing of atmospheric water vapor using the global positioning system," *J. Geophys. Res.*, vol. 97, no. D14, pp. 15787–15801, Oct. 1992.
[26] D. Ji, J. Shi, and S. Zhang, "Water vapor retrieval over cloud cover area on land," in *Proc. 2011 IEEE Int. Geosci. Remote Sens. Symp.* (IGARSS), Jul. 24–29, 2011, pp. 3684–3687. Vancouver, Canada.
[27] K. N. Liou, *An Introduction to Atmospheric Radiation*, 2nd ed., Beijing, China: Meteorological Press, 2004.
[28] T. R. H. Holmes, *The Radiative Temperature of the Earth at Microwave Frequencies*, Amsterdam, the Netherlands: Vrije Universiteit Amsterdam, 2008.
[29] J. C. Shi, T. Jackson, J. Tao, J. Du, R. Bindlish, L. Lu, and K. S. Chen, "Microwave vegetation indices for short vegetation covers from satellite passive microwave sensor AMSR-E," *Remote Sens. Environ.*, vol. 112, no. 12, pp. 4285–4300, Dec. 2008.
[30] T. Wilheit, C. D. Kummerow, and R. Ferraro, "NASDA rainfall algorithms for AMSR-E," *IEEE Trans. Geosci. Remote Sens.*, vol. 41, no. 2, pp. 204–214, Feb. 2003.
[31] T. Wilheit, C. Kummerow, and R. Ferraro, *EOS/AMSR Rainfall Algorithm Theoretical Basis Document,* May 1999. [Online]. Available: Available: http://eospso.gsfc.nasa.gov/sites/default/files/atbd/atbd-amsr-rainfall.pdf.
[32] N. Grody, J. Zhao, R. Ferraro, F. Weng, and R. Boers, "Determination of precipitable water and cloud liquid water over oceans from the NOAA 15 advanced microwave sounding unit," *J. Geophys. Res.*, vol. 106, no. D3, pp. 2943–2953, Feb. 2001.

Dabin Ji received the B.S. and M.Eng. degrees from Shandong University of Science and Technology, Qingdao, China, and the Ph.D. degree from the Chinese Academy of Sciences, Beijing, China, in 2006, 2009, and 2012, respectively.

Then he joined as a Research Assistant in the Institute of Remote Sensing and Digital Earth. His research interest is remote sensing of atmospheric water vapor, cloud, and precipitation.

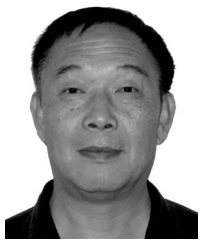

Jiancheng Shi (SM'02–F'14) received the B.A. degree from the University of Lanzhou, Lanzhou, China, and the M.A. and Ph.D. degrees in geography from the University of California, Santa Barbara (UCSB), Santa Barbara, CA, USA, in 1982, 1987, and 1991, respectively.

Then he joined as a Research Scientist in the Institute for Computational Earth System Sciences, UCSB. His research interests are microwave modeling snow and soil signatures, image processing and analysis, and inversion models for retrieving physical parameters from remote sensing data.

Dr. Shi is a Member of the Electromagnetic Academy.